Applied Catalysis B: Environmental 127 (2012) 68–76

Contents lists available at SciVerse ScienceDirect

Applied Catalysis B: Environmental

journal homepage: www.elsevier.com/locate/apcatb

Characterization of thermally treated Co^{2+}-exchanged zeolite X

Hoon Young Jeong[a], Dong-Chan Koh[b], Kwang-Sik Lee[c,*], Hyun Hwi Lee[d,**]

[a] Department of Geological Sciences, Pusan National University, Busan 609-735, South Korea
[b] Geologic Environment Division, Korea Institute of Geoscience & Mineral Resources, Daejeon 305-350, South Korea
[c] Division of Earth and Environmental Science, Korea Basic Science Institute, Ochang, Chungbuk 363-883, South Korea
[d] Pohang Accelerator Laboratory, Pohang University of Science and Technology (POSTECH), Pohang 790784, South Korea

ARTICLE INFO

Article history:
Received 2 March 2012
Received in revised form 20 July 2012
Accepted 2 August 2012
Available online 14 August 2012

Keywords:
Radioactive isotope
Cobalt
Zeolite
EXAFS
SEM

ABSTRACT

This study investigated thermal stabilization of Co^{2+}-exchanged zeolite X (Co—X) using scanning electron microscopy (SEM) coupled with energy dispersive X-ray spectroscopy (EDX), X-ray diffraction (XRD), X-ray absorption spectroscopy (XAS), and leaching tests. From SEM-EDX analysis, cobalt was dispersed randomly at ≤600 °C, suggesting its presence as an extraframework cation in exchange sites. At ≥800 °C, cobalt was locally concentrated with Al on the vitreous surface. Consistent with such observations, XRD data indicated that Co—X maintained the zeolite framework at ≤600 °C, and that it became vitrified and transformed to nepheline ($NaAlSiO_4$(s)) and cobalt aluminate ($CoAl_2O_4$(s)) at ≥800 °C. Cobalt-K edge XAS was subjected to both X-ray absorption near-edge spectroscopy (XANES) and extended X-ray absorption fine structure (EXAFS) analyses. In XANES spectra, the pre-edge peaks and edge-shoulders, characteristic of 4-fold coordinated cobalt (e.g., $CoAl_2O_4$(s)), were not evident at ≤600 °C, but such features were strong at ≥800 °C. The EXAFS spectra of Co—X at ≤600 °C lacked in the coordination shells beyond the first Co—O shell. In contrast, Co—X at ≥800 °C showed the EXAFS spectra similar to $CoAl_2O_4$(s). Taken together, cobalt was likely present as 6-fold coordinated Co^{2+} in exchange sites at ≤600 °C and mainly incorporated into a non-exchangeable $CoAl_2O_4$-like phase in both vitreous and crystalline forms at ≥800 °C. In agreement with this proposition, leaching tests with concentrated $CaCl_2$ solutions supported the greater stability of cobalt at ≥800 °C.

1. Introduction

Nuclear fuel reprocessing and nuclear energy generation produce large amounts of radioactive liquid wastes [1]. Such liquid wastes may contain the radioactive isotope ^{60}Co, one of the most hazardous pollutants present in low-to-intermediate level liquid radioactive wastes [2]. Before disposal, the radioactive cobalt is treated with ion exchangers such as organic resins, clay minerals, and zeolites to prevent it from being introduced into environments [3]. Among them, zeolites are most commonly employed to remove radioactive cations from nuclear wastewaters due to the higher selectivity and capacity for radioactive cations [4] and the greater radiational and thermal stability [5]. Through cation exchange, zeolites sorb radionuclides including $^{60}Co^{2+}$ from nuclear wastewaters [2]. However, the reversible nature of ion exchange makes the once-sorbed nuclides re-exchanged by other cations (Na^+, Ca^{2+}, Mg^{2+}, etc.) in groundwaters [5]. Thus, Co^{2+}-exchanged zeolites are often thermally treated (calcinated) to have radioactive cations in vitreous lattices or non-exchangeable crystalline phases [1,3].

Several mechanisms have been proposed for thermal stabilization of radioactive cations in zeolites. Thermal treatment of zeolites causes dehydration, which in turn results in the redistribution of extraframework cations among different types of exchange sites [6]. The dehydration of zeolite X was found to cause Co^{2+} in site I′ to migrate into site I, the more restricted and less exchangeable site [7]. Thermal treatment also led to the closure of open channels, making sorbed cations no longer available for ion exchange [8]. For example, the melting of the zeolite surface may develop vitreous coating on the surface [3]. These processes account for the increased stability of radionuclides before the whole framework of zeolites breaks down. Upon the collapse of the zeolite framework at higher calcination temperatures, sorbed radionuclides become entrapped within the glassy material or non-exchangeable crystalline phases [1,3]. By thermal treatment, Co^{2+}-exchanged zeolite X was found to transform into cobalt aluminate ($CoAl_2O_4$) along with amorphous phase(s) [1].

Despite the aforementioned stabilization mechanisms, the exact chemical nature of cobalt in thermally treated zeolites has not been fully understood. To date, the structure of Co^{2+}-exchanged zeolites during thermal treatment has been investigated largely based on

* Corresponding author. Tel.: +82 43 240 5337; fax: +82 43 240 5319.
** Corresponding author. Tel.: +82 54 279 1551; fax: +82 54 279 1599.
E-mail addresses: hjeong@pusan.ac.kr (H.Y. Jeong), chankoh@kigam.re.kr (D.-C. Koh), kslee@kbsi.re.kr (K.-S. Lee), hhleec@postech.ac.kr (H.H. Lee).

0926-3373/$ – see front matter © 2012 Elsevier B.V. All rights reserved.
http://dx.doi.org/10.1016/j.apcatb.2012.08.001

Table 1
Physicochemical properties of zeolite X.[a]

Chemical formula	Particle size	Pore size	Bulk density
$Na_{86}Al_{86}Si_{106}O_{384}{\cdot}xH_2O$	125–150 μm	~13 Å	~0.65 g/mL

[a] The data are obtained from the supplier.

XRD method [1,3]. Since XRD is sensitive to the long-range ordering, the information attained by this technique is mostly restricted to the identity of crystalline phases, leading to the incomplete understanding of thermal stabilization mechanisms. Few exceptions have resulted from the structural refinement analysis of XRD data [7,9], by which the local coordination of Co in zeolites can be fully resolved. Yet, most previous studies utilizing such a laborious refinement analysis were not originally intended for thermal treatment of Co^{2+}-exchanged zeolites. Consequently, the calcination temperatures used in those studies were limited, and the experimental conditions were often irrelevant for the purpose of thermal treatment (e.g., heating under vacuum). Furthermore, when the sorbed cobalt becomes associated with or incorporated into amorphous phases during thermal treatment of zeolites, the information on the coordination structure of cobalt cannot be obtained by XRD. The coordination information is necessary given that the stability of sorbed cobalt is determined by the strength of its bonds to the bulk phase(s). In this study, thus, the local coordination structure of cobalt was examined using XAS. Since the XAS signals originate dominantly from a few coordination shells of atoms close to the absorbing atom, it can serve as an effective local structure probe [10]. Besides, SEM and XRD were employed to have the bulk-phase structural information. Leaching tests were also performed to supplement the results from SEM, XRD, and XAS analyses. With these methods, we aimed to investigate the structural changes of Co^{2+}-exchanged zeolites as a function of thermal treatment temperature and time for a better understanding of thermal stabilization mechanisms for cobalt.

Besides the use for the safe disposal of nuclear wastes, zeolites can be effective decontaminants in treating radionuclide-contaminated sites [11,12] or back-fill materials in nuclear waste repositories [13]. In such applications, zeolites tend to receive great amounts of heat and radiation dose, both of which gradually amorphorize zeolites over time [8]. Even before the complete amorphorization of zeolites, sorbed radionuclides were found to be more stabilized [14]. Nonetheless, most previous researches have been mainly focused on the thermal stabilization of sorbed radionuclides in zeolites at temperatures at which amorphorization occurs. Thus, it was also our goal to examine the structure of thermally exposed, yet crystalline zeolites for the prediction of the stability change of cobalt over a wide range of temperatures.

2. Experimental

2.1. Sample preparation

Zeolite X, a synthetic Al-rich zeolite with the faujasite framework [15], was purchased from Sigma–Aldrich (see Table 1 for its physicochemical properties and Fig. A.1 in Supplementary Material for the structure). The zeolite powder was pretreated as follows: 100 g of the powder was equilibrated with 1000 mL of 5 M NaCl solution for 7 days, after which it was washed out with deionized water several time to remove the residual NaCl and oven-dried at 60 °C. To prepare Co^{2+}-exchanged form (Co—X), the pretreated sample (80 g) was reacted at pH ~ 6.3 with 1000 mL of 0.32 M $CoCl_2$ solution for 48 h on a magnetic stirrer. The slightly acidic condition in preparing Co—X was chosen to prevent the precipitation of $Co(OH)_2(s)$ and minimize the exchange of proton for Na^+ in zeolite [7]. Following the exchange of Co^{2+} for Na^+, the resultant sample was thoroughly rinsed with deionized water to remove the residual $CoCl_2$ and then oven-dried at 60 °C. A portion of Co—X samples was digested with a mixture of nitric, hydrofluoric, and perchloric acids at 200 °C for overnight, and then was analyzed for the composition of Na, Co, and Al using an Inductively Coupled Plasma-Atomic Emission Spectrometer (ICP-AES). Approximately 58% of the total exchange sites in Co—X were found to be occupied by Co^{2+}, with the resultant unit formula of $Na_{36}Co_{25}Al_{86}Si_{106}O_{384}$. Such incomplete Co^{2+} occupancy has been previously observed for zeolite X [7].

Co—X samples were thermally treated using a chamber furnace with a SiC rod (Nabertherm, Inc.) under the atmosphere. The furnace temperature was ramped at a rate of 20 °C/min and kept isothermal at the target treatment temperatures (400, 600, 800, 1000, and 1200 °C) for 2–24 h. Such treatment conditions covered where the zeolite structure was retained and collapsed. The similar temperatures were previously employed in thermal treatment of Co^{2+}-exchanged zeolite X [1]. After thermal treatment, the samples were quickly removed from the furnace and allowed to quench at room temperature. Prior to use, thermally treated samples were stored inside air-tight serum vials to prevent the absorption of moisture from the atmosphere. As described in the following sections, the samples were subjected to leaching tests as well as solid-phase characterization using SEM, XRD, and XAS techniques.

2.2. SEM and XRD

The effect of thermal treatment on the size and morphology of particles and the distribution of elements was examined using a scanning electron microscope (HITACHI 6853-H) equipped with an energy dispersive X-ray spectroscope at voltages of 5–15 kV. Sample powders were applied on a conductive carbon tape and then coated with a Pt film. Image processing and analysis were performed using ImageJ 1.42 (National Institutes of Health, USA).

XRD provides information on changes of the crystallinity and mineralogical composition of Co—X by thermal treatment. Each powder sample was loaded into a quartz capillary. X-ray diffraction measurements were performed with an 18 keV X-ray beam at beamline 5A at Pohang Accelerator Laboratory (PAL). Diffraction patterns were recorded on a MAR345 image plate, and the data were then processed using the Fit2d suite [16]. For the samples maintaining the zeolite framework, the unit cell parameter was extracted from the reflection peak positions.

2.3. XAS

Cobalt-K edge XAS spectra were collected at ambient temperature at beamline 10B (2.5 GeV, ~150 mA) at PAL using an unfocused beam with a Si(1 1 1) double-crystal monochromator. Transmission and fluorescence signals were simultaneously measured using high precision ionization chambers (IC-SPEC) and a bent crystal Laue analyzer, respectively. The monochromator was detuned at minimum 50% at the highest energy of the scan to reject the contribution from high-order harmonics. The beam energy was calibrated for each scan using a Co foil at Co-K edge (7709 eV). XAS spectra were obtained for both thermally treated samples and reference compounds including aqueous $Co^{2+}(aq)$, $Co(OH)_2(s)$, and $Co_3O_4(s)$. The aqueous Co^{2+} was prepared by dissolving $Co(NO_3)_2$ salt in water to have the resultant Co concentration of 0.1 M. Four to nine scans were collected to enhance the signal-to-noise ratios. The XAS spectrum of cobalt aluminate ($CoAl_2O_4(s)$) was provided by Maurizio et al. [17].

XAS analysis was performed using SixPACK [18]. Individual scans were averaged, and the background absorbance was removed by a linear fit through the pre-edge region. X-ray absorption

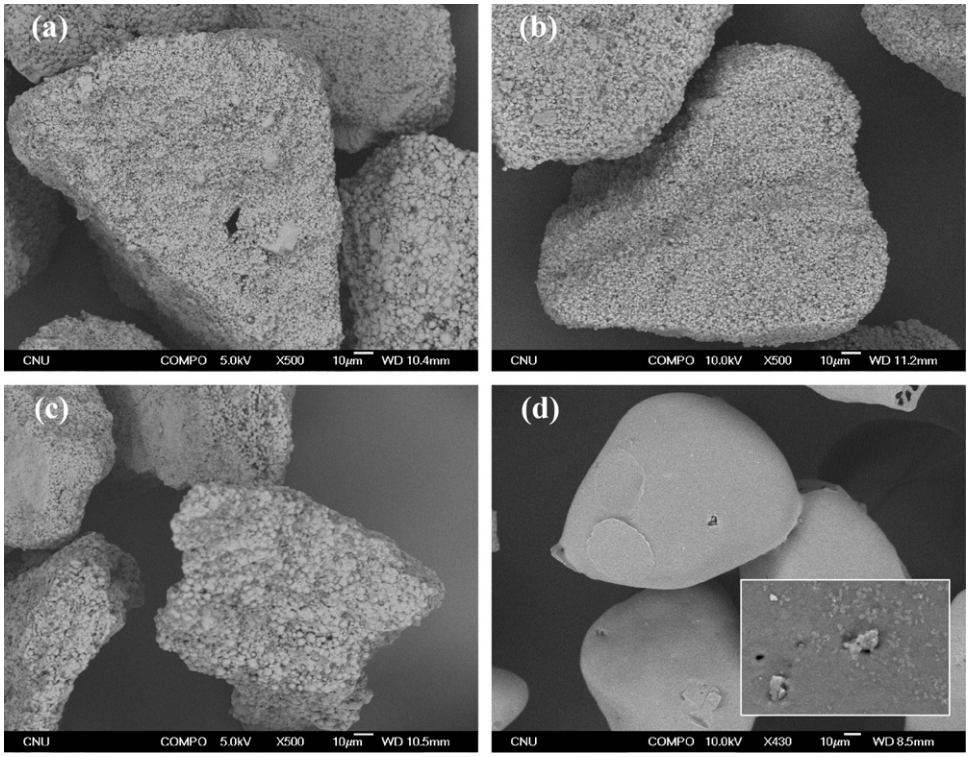

Fig. 1. SEM images of Co^{2+}-exchanged zeolite X: thermally untreated sample (a) and the samples treated at 600 (b), 800 (c), and 1000 °C (d) for 2 h. In part (d), a close-up image of the particle surface is inserted. Scale bars are located at the bottom of each image.

near-edge structure (XANES) spectra (7700–7760 eV) were isolated by normalizing the signal to the edge-jump height. Extended X-ray absorption fine structure (EXAFS) spectra were obtained by fitting a quadratic spline function above the absorption edge. EXAFS spectra were normalized using a Victoreen polynomial function and then converted from energy to frequency space (k-space) using an E_0 of 7720 eV. The resultant spectra ($\chi(k)$) were weighted by k^3 to amplify the higher k-range, and Fourier-transformed to produce radial structure functions (RSFs) in R space over a k range of 3.0–12.0 $Å^{-1}$. The first shells corresponding to the Co—O path in R space were back-transformed to produce filtered EXAFS spectra to determine their contribution to the overall spectra. Least-squares fitting of k^3-weighted EXAFS functions ($k^3\chi(k)$) was performed using the phase and amplitude functions derived from $CoAl_2O_4$(s) using FEFF 8 [19] to estimate structural parameters. After optimized from the fitting of the reference spectra, the amplitude-reduction factor (S_0^2) was constrained at 0.9 for all data analysis. Then, using the filtered EXAFS spectra, the Debye–Waller factors (σ^2) of the first coordination shells (e.g., Co—O interactions) were optimized by increment of 0.0005. Using the raw EXAFS spectra, the σ^2 values of additional shells were subsequently optimized either for individual sample spectra or as groups among the sample spectra exhibiting the similar patterns. During the fitting, other parameters including coordination number (N), bond distance (R), and energy shift (ΔE_0) were allowed to vary. In case of energy shift, a single value was assigned to fit all absorber-backscatter pairs in a sample. The best fit was obtained by minimizing the goodness of fit parameter (R_f) [18]. The resultant R and N for the first shells were estimated to be accurate within ±0.02 Å and ±20%, respectively [20].

2.4. Leaching tests

To assess the effect of thermal treatment on the stability of sorbed Co^{2+}, 1.5 g of thermally treated Co—X samples were added to 25 mL of 0.4 M $CaCl_2$ solution in 50 mL centrifuge tubes. Then, the tubes were shaken over an end-over-end rotor for 2 weeks. In our preliminary tests, this period was sufficient to reach equilibrium. Ca^{2+} was chosen since it comprises the major dissolved cations in groundwaters [21], and Al-rich zeolites including zeolite X have a marked preference for divalent cations over monovalent cations [4]. At the end of leaching experiments, filtrates were obtained by passing the solutions through 0.2 μm syringe-filters and analyzed for the aqueous Co using an ICP-AES. The pH measured after the equilibrium period ranged between 7.2 and 8.3. Possible causes for the pH variation would be the hydrolysis of the liberated Co^{2+} and the dissolution of Co—X and its calcination products.

3. Results and discussion

3.1. SEM analysis

The SEM images of thermally treated Co—X are shown in Fig. 1. The untreated sample (Fig. 1(a)) consists of angular particles with highly porous and rough surfaces. Relative to the untreated one, the sample treated at 600 °C (Fig. 1(b)) has less rough surfaces. The 800 °C-treated sample (Fig. 1(c)) shows a distinct surface texture, which is marked by the development of pimple-like projections. Such a texture would result from the partial melting of the surface. At 1000 °C (Fig. 1(d)), particles are characterized by the glassy texture. The similar feature was previously reported in thermally treated zeolite Y, and it was attributed to the vitrification of zeolite Y [8]. In the inserted image of Fig. 1(d), fine grains with size of <~2 μm protrude from the vitreous surface, indicating the development of secondary phases from the underlying glassy material.

Fig. 2 compares the EDX maps between the untreated sample and that treated at 1000 °C. In case of the untreated sample, Al, Si, and Co are dispersed at nearly random (see Fig. 2(a) for EDX maps and the related analysis for Fig. A.2 in Supplementary Material), which is in line with the presence of cobalt as a charge-balancing cation in exchange sites. In the meanwhile, the sample treated

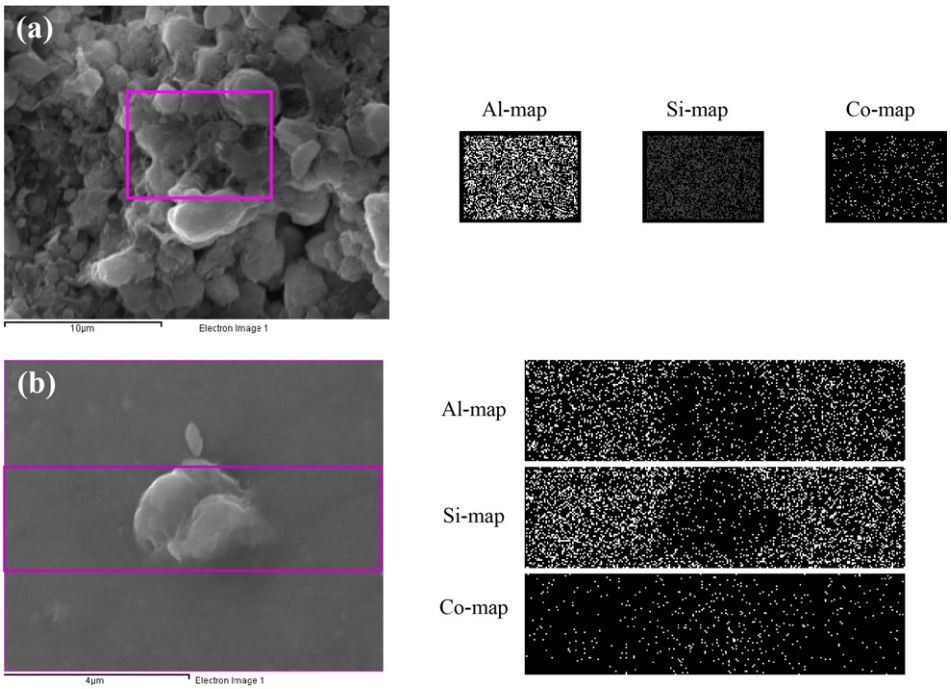

Fig. 2. SEM images and the corresponding EDX maps of Al, Si, and Co for thermally untreated sample (a) and the sample treated at 1000 °C for 2 h (b). Note that the EDX maps are constructed for the boxed areas in the images. Refer to Fig. A.2, Supplementary Material for the detailed analysis.

at1000 °C displays more spatially varied distributions of the elements (see Fig. 2(b)). Where the protruding grains are present, the intensity ratios of Al and Co to Si are substantially increased (see Fig. A.2 in Supplementary Material), suggesting the formation of secondary phases enriched with Al and Co. As later discussed in XRD and XAS analyses, this secondary phase is likely $CoAl_2O_4$(s). Besides, the lower intensity ratio of cobalt is noted outside the protruding grains, pointing to the incorporation of Co into the bulk glassy phase. Previously, by thermal treatment of Co—X, cobalt was proposed to be occluded in the amorphous phase or incorporated into $CoAl_2O_4$(s) [22]. Consistent with such proposition, our EDX data support the presence of cobalt in both vitreous and crystalline phases at higher treatment temperatures.

The particle size of thermally treated Co—X was determined from SEM images in Fig. A.3, Supplementary Material. The mean diameters of the untreated sample and those treated at 600, 800, and 1000 °C for 2 h are 134, 131, 114, and 112 mm, respectively. The decreased particle size with the higher treatment temperature was caused by the removal of extraframework water and the collapse of open channels by thermal treatment.

3.2. XRD analysis

Thermal effect on the crystal structure of Co—X as well as the formation of secondary phases was examined using XRD. Fig. 3 shows the diffraction patterns of Co—X as a function of thermal treatment temperature and time. Co—X retains the faujasite framework up to 600 °C, but it undergoes the complete transformation to several crystalline phases as well as the glassy material at ≥800 °C. The temperature where amorphorization occurs is strongly affected by the type of extraframework cations [3]. When Na^+ is exchanged by larger cations (e.g., Cs^+), SiO_4 tetrahedra in the zeolite framework are stabilized [7]. For example, compared to the fully Na^+-exchanged zeolite Y (Na—Y), a partially Cs^+-substituted Na—Y needed a higher amorphorization temperature [8]. In contrast, when Na^+ is exchanged by smaller cations (e.g., Co^{2+}), the tetrahedra are destabilized [7]. Previously, the partial exchange of Co^{2+} for Na^+ in zeolite X was found to lower the amorphorization temperature [3]. Despite the significant difference in the Co contents, our Co—X sample (25.8 mequivalent/g) shows the similar amorphorization temperature to that prepared by Bulbulian and Bosch [1] (0.86 mequivalent/g), indicating that the amorphorization temperature of zeolite X is rather insensitive to the amount of exchanged Co^{2+}.

Among the samples retaining the faujasite framework, the position of reflection peaks changes with the treatment temperature. From the insert of Fig. 3(a), the position of the (1 1 1) peak at ~14.5 Å shifts to lower d values by thermal treatment. Based on the cubic symmetry (i.e., $a = b = c$), the unit cell parameter was determined to be 24.90 ± 0.03 Å for the untreated sample, 24.81 ± 0.02 Å for the sample treated at 400 °C for 2 h, and 24.79 ± 0.01 Å for that at 600 °C for 2 h. The shortest unit cell parameter observed here is larger than that reported for a fully dehydrated Co^{2+}-exchanged zeolite X (24.597 Å from Borissenko et al. [7]). The decreased unit cell parameter was due to the dehydration.

Thermal treatment also affects the intensity of the reflection peaks of Co—X. By thermal treatment, the intensity of the (1 1 1) peak increases, but that of the (2 2 0) peak at ~8.8 Å decreases. This feature cannot be explained by the dehydration alone, which would lead to the change of the peak intensities in a uniform fashion. Previously, Borissenko et al. [7] have postulated that both the redistribution of Co^{2+} among different exchange sites and the dehydration during thermal treatment strengthen the electrostatic interaction between Co^{2+} and the framework oxygen, resulting in the distortion of the framework geometry. Similarly, Lima et al. [22] reported the structural distortion of tetrahedral aluminum (AlO_4) using ^{27}Al MAS NMR. Accordingly, both the migration of Co^{2+} and the dehydration would promote the local distortion of the zeolite framework, resulting in the observed crystallographic axis-dependent change in the peak intensities.

In Fig. 3(b), it is evident that the zeolite framework completely breaks down to form glassy material and secondary phases by thermal treatment at ≥800 °C. The vitrification of Co—X and the recrystallization of secondary phases are consistent with the

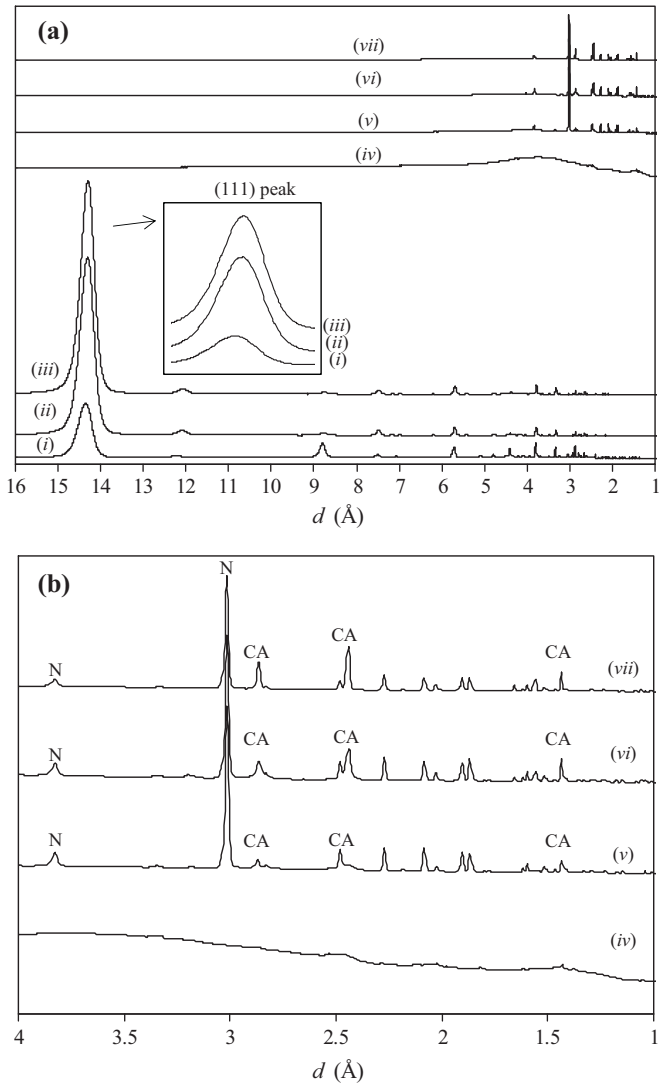

Fig. 3. XRD patterns of Co^{2+}-exchanged zeolite X: thermally untreated sample (*i*) and the samples treated at 400 °C for 2 h (*ii*), 600 °C for 2 h (*iii*), 800 °C for 2 h (*iv*), 800 °C for 24 h (*v*), 1000 °C for 2 h (*vi*), and 1200 °C for 2 h (*vii*). In part (a), the (1 1 1) reflection peak of zeolite is enlarged to visualize changes in its location. The reflection peaks at $d < 4$ Å are presented for the samples treated at ≥800 °C in part (b), where some peaks are indexed for cobalt aluminate ($CoAl_2O_4$(s), CA) and nepheline ($NaAlSiO_4$(s), N), with the other peaks unidentified despite intensive searches.

SEM observation that small grains develop on the vitreous surface (see the inserted image in Fig. 1(d)). Some reflection peaks at ≥800 °C match those of cobalt aluminate ($CoAl_2O_4$(s)) and nepheline ($NaAlSiO_4$(s)). Of the two, cobalt aluminate likely corresponds to the protruding grains enriched with Al and Co in Fig. 2(b). Similar to zeolites, the charge-balancing cations in nepheline are also prone to ion exchange [1]. As later discussed in leaching tests, little liberated Co^{2+} in the samples treated at ≥800 °C rebuts the presence of Co^{2+} in nepheline as the charge-balancing cation. Considering the high Co content (25.8 mequivalent/g) in this study, cobalt oxides including CoO and Co_3O_4 were expected to form as Co—X became dehydrated by thermal treatment [23]. However, no crystalline cobalt oxides were observed by XRD. Yet, since cobalt is found to be incorporated into the glassy material from the EDX analysis, the possibility that Co^{2+} is present as amorphous cobalt oxides cannot be ruled out at this point.

3.3. XAS analysis

The local coordination structure of cobalt was investigated using Co-K edge XAS, which was subjected to XANES and EXAFS analyses. While the former provides the qualitative information on the coordination structure, the latter provides the quantitative information.

The XANES spectra of thermally treated Co—X are presented in Fig. 4, where those of reference compounds are also included for comparison. In the raw XANES spectra and the first derivatives, the untreated sample and those treated at ≤600 °C show the similar patterns to aqueous Co^{2+}. Nonetheless, the variation in the white line and absorption edge energy is noted among these samples. Compared to the untreated sample, those treated at ≤600 °C show the weaker white line (a sharp intensive peak at the rising absorption edge). The decreased white line was attributed to the removal of extraframework water [24]. The absorption edge energy, determined by the first maximum in the derivative of XANES spectra, decreases with the treatment temperature (e.g., 7719.0 eV for both the untreated sample and those treated at 400 °C; 7718.0 eV for the samples treated at 600 °C). While Co^{2+} in ionic states (e.g., 7720.5 eV for $CoCl_2{\cdot}6H_2O$(s)) has a higher absorption edge energy, Co^{2+} in covalent states (e.g., 7717.2 eV for CoO(s)) has a lower energy [25]. In this study, the absorption edge energy of Co^{2+}-containing reference compounds is found to decrease with the higher covalency (e.g., 7719.5 eV for aqueous Co^{2+}, 7719.0 eV for $Co(OH)_2$(s), and 7717.3 eV for $CoAl_2O_4$(s)). Thus, the observed lower absorption edge energy at higher treatment temperatures points to the greater covalent character in the coordination environment of Co.

In Fig. 4, the XANES spectra (especially the first derivatives) of the samples treated at ≥800 °C are significantly different from those of the samples treated at ≤600 °C. Notably, those treated at ≥800 °C have the pre-edge peak at ~7709.5 eV (indicated by *i*). The pre-edge peak arises from the electron transition from 1s orbital to 3d orbital in tetrahedrally coordinated Co^{2+} [26]. In Fig. 4, the samples treated at ≥800 °C also exhibit the distinct shoulders just above the edge jump (indicated by *ii*), which are also characteristic of tetrahedrally coordinated Co^{2+} [17]. While Co_3O_4(s) consists of 1/3 of tetrahedrally coordinated Co^{2+} and 2/3 of octahedrally coordinated Co^{3+}, $CoAl_2O_4$(s) contains only tetrahedrally coordinated Co^{2+}. Thus, due to the higher occupancy of Co^{2+} in tetrahedral sites, $CoAl_2O_4$(s) displays the stronger pre-edge peak and edge-shoulders than Co_3O_4(s) (see Fig. 4). Previously, the calcination of Co^{2+}-exchanged zeolites was found to produce CoO(s) and/or Co_3O_4(s) [23,25]. Since CoO(s) has all octahedrally coordinated Co^{2+} [17], it should lack in the pre-edge peak and edge-shoulders. Also, the weak pre-edge peak and edge-shoulders in Co_3O_4(s) contrast with their strong features in the samples treated at ≥800 °C. Furthermore, the absorption edge energy of Co_3O_4(s) (7719.0 eV) is much higher than those treated at 1000 and 1200 °C (7717.1 eV), which are close to that of $CoAl_2O_4$(s) (7717.3 eV). By thermal treatment at ≥800 °C, thus, the possibility that cobalt crystallizes as amorphous cobalt oxides is eliminated; instead, cobalt is more likely to be incorporated into a $CoAl_2O_4$(s)-like phase. Given the SEM-EDX analysis in Fig. 2(b) and the XRD pattern in Fig. 3(b), such a phase would likely take both vitreous and crystalline forms.

Fig. 5 shows the Co-K edge EXAFS spectra and the corresponding Fourier transforms of reference compounds as well as Co—X samples. Table 2 summarizes the structural parameters obtained by the numerical fitting. The untreated sample and those treated at ≤600 °C have the EXAFS spectra dominated by the Co—O bond in the first coordination shell (see Fig. 5(b)). Also, these samples exhibit the weak second coordination shells, in contrast to the strong second coordination peaks observed in well-ordered Co-containing minerals such as $Co(OH)_2$(s), $CoAl_2O_4$(s), and Co_3O_4(s) (see Fig. 5(b)). Given the relatively disordered nature in the

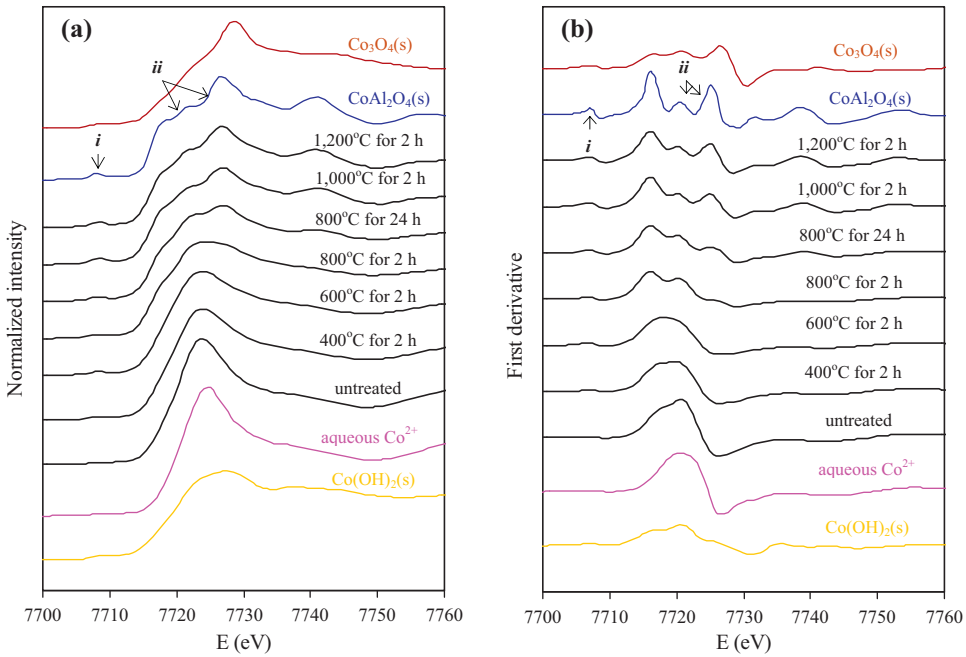

Fig. 4. Co-K edge XANES spectra (a) and the first derivatives (b) for Co^{2+}-exchanged samples as well as reference compounds. With enveloped by reference compounds, the samples (all in black) are arranged from bottom to top as follows: thermally untreated sample, the samples treated at 400 °C for 2 h, 600 °C for 2 h, 800 °C for 2 h, 800 °C for 24 h, 1000 °C for 2 h, and 1200 °C for 2 h. Pre-edge peaks and shoulders at the edge jump are indicated by *i* and *ii*, respectively.

interaction between the extraframework cobalt and the framework Al or Si (i.e., Co—Al/Si) in exchange sites, thus, cobalt would be a charge-balancing cation in the untreated sample and those treated at ≤600 °C.

According to the bond-valence principle [27], the bond distance should decrease with the lower coordination number to compensate for the weakened bond strength. In agreement with this principle, $CoAl_2O_4$(s), which contains tetrahedrally coordinated Co^{2+} [17], is found to have the shorter Co—O bond than aqueous Co^{2+} and $Co(OH)_2$(s), in which Co^{2+} is octahedrally coordinated [10] (see Fig. 5(b) and Table 2). The Co—O bond distances in the untreated sample and those treated at ≤600 °C (2.05–2.07 Å) are much longer than that of $CoAl_2O_4$(s) (1.97 Å) but comparable to those of aqueous Co^{2+} (2.08 Å) and $Co(OH)_2$(s) (2.10 Å), suggesting the 6-fold coordination for Co in these samples. Indeed, the numerical fitting of EXAFS spectra reveals that the thermally untreated

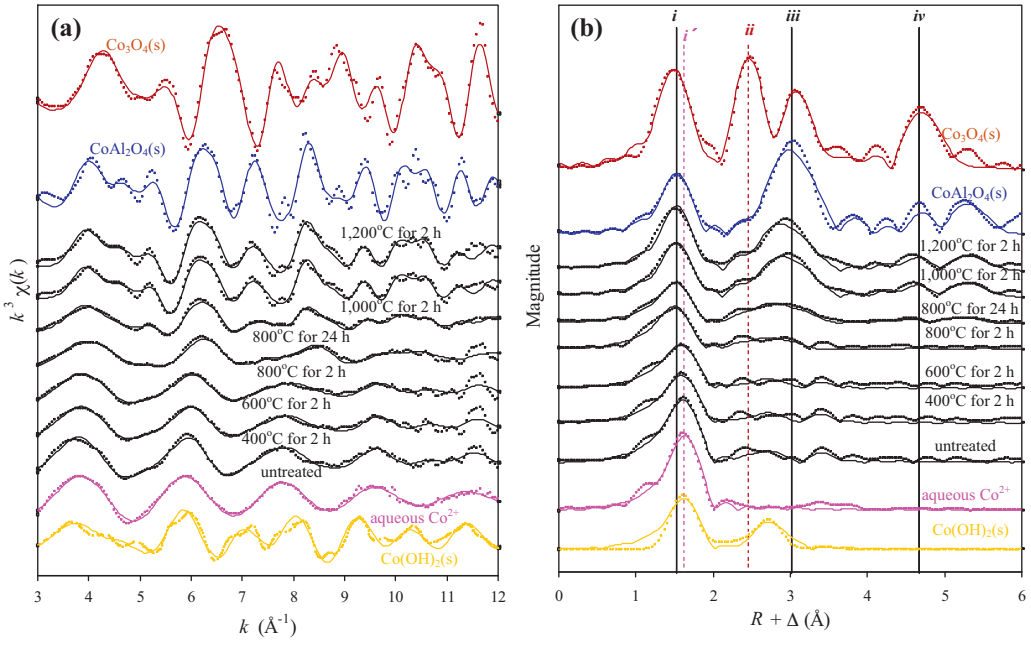

Fig. 5. k^3-Weighted Co-K edge EXAFS spectra ($k^3\chi(k)$) (a) and the corresponding Fourier transforms (b) of Co^{2+}-exchanged samples as well as reference compounds. With enveloped by reference compounds, the samples (all in black) are arranged from bottom to top as follows: thermally untreated sample, the samples treated at 400 °C for 2 h, 600 °C for 2 h, 800 °C for 2 h, 800 °C for 24 h, 1000 °C for 2 h, and 1200 °C for 2 h. Dashed lines represent the experimental data, and solid lines are the numerical fits. In part (b), lines *i*, *i′*, and *ii* represent the positions of the Co—O bond in the samples treated at ≥800 °C, the Co—O bond in the samples treated at ≤600 °C, and the Co—Co bond among the octahedrally coordinated Co in Co_3O_4(s), respectively. Also, lines *iii* and *iv* correspond to the second and third coordination shells of the samples treated at ≥800 °C. Note that peak positions in part (b) are uncorrected for phase shift.

Table 2
EXAFS fit results for reference compounds and thermally treated Co^{2+}-exchanged zeolite X.[a]

Sample	Pair	N	R (Å)	σ^2 (Å^2)	Sample	Pair	N	R (Å)	σ^2 (Å^2)
Aqueous Co^{2+}	Co—O	6.2	2.08	0.007	$Co(OH)_2$(s)	Co—O	6.0	2.10	0.0065
	$\Delta E_0 = -9.66$ eV, $R_f = 0.029$					Co—Co	5.8	3.17	0.0045
						Co—Co	6.1	6.34	0.0045
						$\Delta E_0 = -8.51$ eV, $R_f = 0.058$			
Co_3O_4(s)	Co—O	5.2	1.91	0.004	$CoAl_2O_4$(s)	Co—O	4.0	1.97	0.004
	Co—Co	3.4	2.85	0.003		Co—Al	10.0	3.30	0.005
	Co—Co	4.2	3.36	0.003		Co—O	12.0	3.32	0.009
	Co—Co	8.4	5.29	0.003		Co—Co	5.0	3.51	0.004
	$\Delta E_0 = -9.68$ eV, $R_f = 0.101$					Co—O	12.0	4.34	0.009
						Co—Al	12.0	5.32	0.004
						Co—Co	12.0	5.71	0.005
						$\Delta E_0 = -7.26$ eV, $R_f = 0.139$			
Untreated	Co—O	6.1	2.07	0.0085					
	Co—Al/Si	1.1	3.26	0.0045					
	Co—Al/Si	1.5	3.83	0.0045					
	$\Delta E_0 = -11.80$ eV, $R_f = 0.051$								
400 °C	Co—O	5.0	2.06	0.0095	600 °C	Co—O	5.0	2.05	0.01
for 2 h	Co—Al/Si	0.9	3.25	0.003	for 2 h	Co—Al/Si	0.8	3.25	0.003
	Co—Al/Si	1.1	3.82	0.003		Co—Al/Si	0.7	3.81	0.003
	$\Delta E_0 = -11.37$ eV, $R_f = 0.107$					$\Delta E_0 = -11.29$ eV, $R_f = 0.089$			
800 °C	Co—O	3.7	1.97	0.008	800 °C	Co—O	3.1	1.98	0.007
for 2 h	Co—Al	1.6	3.20	0.008	for 24 h	Co—Al	2.5	3.22	0.008
	Co—Co	0.5	3.40	0.008		Co—Co	1.6	3.48	0.008
	Co—Al	1.0	5.39	0.008		Co—Al	3.3	5.27	0.008
	Co—Co	0.6	5.78	0.008		Co—Co	3.0	5.68	0.008
	$\Delta E_0 = -14.78$ eV, $R_f = 0.088$					$\Delta E_0 = -12.63$ eV, $R_f = 0.047$			
1000 °C	Co—O	2.9	1.97	0.004	1200 °C	Co—O	3.4	1.97	0.004
for 2 h	Co—Al	4.2	3.27	0.008	for 2 h	Co—Al	5.3	3.28	0.005
	Co—Co	3.5	3.50	0.008		Co—Co	3.6	3.51	0.009
	Co—Al	9.8	5.31	0.008		Co—Al	11.0	5.32	0.005
	Co—Co	7.8	5.71	0.008		Co—Co	8.3	5.73	0.009
	$\Delta E_0 = -9.65$ eV, $R_f = 0.069$					$\Delta E_0 = -9.08$ eV, $R_f = 0.083$			

[a] The amplitude-reduction factor (S_0^2) is set at 0.9; ΔE_0 and R_f indicate energy shift and goodness of the fit, respectively.

sample and those treated at ≤600 °C have the Co—O bonds with the coordination number of ~6 (see Table 2). Furthermore, the Co—O bond distances in these samples are even longer than those of Co^{3+}-containing phases such as Co_3O_4(s) (1.91 Å in this study) and Co^{3+} species (~1.82 Å from Verberckmoes et al. [28]). Taken together, cobalt in the thermally untreated sample and those treated at ≤600 °C is mainly 6-fold coordinated Co^{2+}.

For untreated, hydrated zeolite X, Co^{2+} in exchange site I is coordinated by six framework oxygens (i.e., $Co(Ox)_6^{2+}$ where Ox represents the framework oxygen), and Co^{2+} in sites I′ and II is coordinated by three lattice oxygens and three water molecules (i.e., $Co(Ox)_3(H_2O)_3^{2+}$) (refer to Fig. A.1 in Supplementary Material for the location of different exchange sites) [28]. However, thermal treatment of zeolite X removes water molecules from Co^{2+} in sites I′ and II, leaving it as $Co(Ox)_3H_2O^{2+}$ (tetrahedral form) or $Co(Ox)_3^{2+}$ (trigonal form), with the 6-fold coordination retained for Co^{2+} in site I [26,28]. In this regard, the near 6-fold coordination for Co^{2+} during thermal treatment at ≤600 °C was probably due to the migration of Co^{2+} from sites I′ and II to site I. Previously, the relocation of Co^{2+} in favor of site I during dehydration of zeolite X was observed by Borissenko et al. [7]. In this study, the redistribution of Co^{2+} among different sites would have to occur quickly in that the similar phenomenon took six to seven days in the experiments conducted by Borissenko et al. [7]. Our Co—X samples maintaining the zeolite framework were thermally treated at 400–600 °C, whereas their samples were thoroughly evacuated under vacuum at room temperature or 400 °C. Such variations in the experimental procedures would make different migration rates of Co^{2+}.

Since 16 sites I are available per unit cell of zeolite X [6], the maximum of 16 Co^{2+} per unit cell ($Na_{36}Co_{25}Al_{86}Si_{106}O_{384}$) reside in site I, rendering the simultaneous occupation of site I′ impossible due to the strong repulsion between two neighboring Co^{2+} in sites I and I′. Yet, the remaining 9 Co^{2+} ions per unit cell are likely to sit in site II, where Co^{2+} would have 3- or 4-fold coordination by dehydration. However, a recent structure refinement study of a fully dehydrated zeolite X [7] has revealed that even Co^{2+} ions in site II bind to 6 framework oxygens as a result of the distortion of local framework structure. Taken together, either the redistribution of Co^{2+} among different exchange sites, or the local structural distortion, or both are responsible for the near 6-fold coordination of Co^{2+} during thermal treatment at ≤600 °C.

In Table 2, the samples treated at ≥800 °C have the lower coordination number of the Co—O bonds than those treated at ≤600 °C. One may argue that the decreased coordination number results from the intensive dehydration of the extraframework Co^{2+} in sites I′ and II, which makes Co^{2+} tetrahedrally or trigonally coordinated. However, since at dehydrated states the majority of Co^{2+} is preferentially placed in site I (where Co^{2+} is octahedrally coordinated), the view of Co^{2+} as a charge-balancing cation in the exchange sites is not an appropriate account for the observed lower coordination number in the samples treated at ≥800 °C. In Table 2, the samples treated at ≥800 °C have the Co—O bond at ~1.97 Å, which is significantly shorter than the Co—O distance of the samples treated at ≤600 °C but close to that of $CoAl_2O_4$(s). This feature is also evident in Fig. 5(b), where the first coordination shells of the samples treated at ≥800 °C as well as $CoAl_2O_4$(s) (peak *i*) are located at lower *R* than those of the samples treated at ≤600 °C (peak *i*′). The samples treated at ≥800 °C exhibit additional coordination shells at longer *R*: the second shell at 3.20–3.51 Å (denoted by peak *iii* in Fig. 5(b)) and the third shell at 5.27–5.78 Å (denoted by peak *iv* in Fig. 5(b)), both of which are weak or absent in the samples treated at ≤600 °C. These higher coordination shells become stronger with the increasing treatment temperature and time, indicating the progressive development of a long-range-ordered Co-containing phase. In fact,

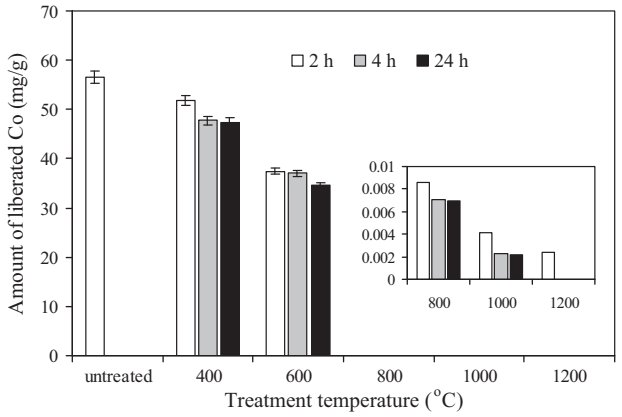

Fig. 6. Amount of the liberated Co as a function of thermal treatment temperature and time in leaching tests with Ca^{2+}. Error bars represent one standard deviation.

the EXAFS spectra and radial structure functions (RSFs) of the samples treated at ≥800 °C resemble those of $CoAl_2O_4$(s). As in case of $CoAl_2O_4$(s), the second shells of those treated at ≥800 °C are characterized by a single peak *iii*, which contrasts with the presence of two peaks *ii* and *iii* in the second coordination shells of Co_3O_4(s). Also, taking into account the strong pre-edge peak and edge-shoulders in the XANES spectra, cobalt in the samples treated at ≥800 °C is thought to be manly incorporated into a $CoAl_2O_4$(s)-like phase.

As previously mentioned, a $CoAl_2O_4$(s)-like phase is present in both vitreous and crystalline states. The relative importance of both states is strongly affected by the treatment temperature and time. The stronger reflection peaks in Fig. 3(b) with the treatment temperature and time indicate the increased crystallinity of a $CoAl_2O_4$(s)-like phase. Also, the second and third coordination shells (e.g., peaks *iii* and *iv* in Fig. 5(b)), indicative of the long-range order, become more evident with the treatment temperature and time.

3.4. Leaching tests

Fig. 6 describes the liberated Co amount as a function of treatment temperature and time to assess the effectiveness of thermal treatment. In Fig. 6, thermal treatment at ≤600 °C is found to reduce the Co^{2+} leaching. Although the zeolite structure is retained at ≤600 °C, the migration of Co^{2+} to the less exchangeable site I and/or the local disturbance of the open-channel network within zeolites would make Co^{2+} less available for exchange with Ca^{2+}. In Fig. 6, the Co^{2+} leaching is markedly decreased by thermal treatment at ≥800 °C, at which the vitrification of Co—X and the formation of secondary crystalline phases (e.g., nepheline and cobalt aluminate) take place. Given the reversible nature in the sorption of charge-balancing cations in nepheline [1], the very low leaching in the samples treated at ≥800 °C suggests that cobalt is unlikely to be trapped in the nepheline phase. Instead, cobalt is mainly incorporated in a non-exchangeable $CoAl_2O_4$(s)-like phase by thermal treatment at ≥800 °C.

4. Conclusions

This study investigated the bulk structure and coordination chemistry of thermally treated Co—X. The experimental results provide the mechanistic insights into the thermal stabilization of cobalt below and above the amorphorization temperature of Co—X. By thermal treatment at ≤600 °C, Co—X is found to maintain the zeolite framework, with several key features noted as follows:

- In SEM-EDX maps, a rather random distribution of cobalt is indicative of the presence of cobalt as a charge-balancing cation in exchange sites.
- From XRD analysis, the position and intensity of the reflection peaks of Co—X are changed due to the dehydration and the resultant structural change during thermal treatment.
- From XAS analysis, cobalt is likely to be present as a charge-balancing cation with the near 6-fold coordination.
- The decreased Co leaching with the treatment temperature results from the greater covalence due to the redistribution of Co^{2+} among different exchange sites and/or the local structural distortion of Co—X.

In contrast, thermal treatment at ≥800 °C leads to the complete vitrification of Co—X and the subsequent recrystallization of secondary phases:

- From SEM-EDX analysis, the protruding grains are enriched with Co and Al, with the underlying vitreous phase characterized by the relatively low Co content.
- By XRD analysis, the cobalt-rich grains prove to be essentially $CoAl_2O_4$(s).
- From XAS analysis, cobalt is mainly present as a $CoAl_2O_4$(s)-like phase in both vitreous and crystalline forms.
- The very low Co leaching is consistent with the incorporation of cobalt into a non-exchangeable $CoAl_2O_4$(s) phase.

Acknowledgements

We thank Dr. Chiara Maurizio for providing the XAS spectrum of $CoAl_2O_4$(s) and Dr. Yongjae Yu for collecting SEM images. This research was supported by Basic Science Research Program through the National Research Foundation of Korea (NRF) funded by the Ministry of Education, Science and Technology (2010-0023824) and the NAP (National Agenda Project) of the Korea Research Council of Fundamental Science & Technology. Experimental works at Pohang Accelerator Laboratory (PAL) were supported in part by Ministry of Educational Science and Technology of the Korean Government and Pohang University of Science and Technology (POSTECH).

Appendix A. Supplementary data

Supplementary data associated with this article can be found, in the online version, at http://dx.doi.org/10.1016/j.apcatb.2012.08.001.

References

[1] S. Bulbulian, P. Bosch, Journal of Nuclear Materials 295 (2001) 64–72.
[2] I. Smičiklas, S. Dimović, I. Plećaš, Applied Clay Science 35 (2007) 139–144.
[3] R. Rodríguez-Trejo, P. Bosch, S. Bulbulian, Journal of Nuclear Materials 354 (2006) 110–122.
[4] C. Colella, Mineralium Deposita 31 (1996) 554–562.
[5] A. Dryer, An Introduction to Zeolite Molecular Sieves, John Wiley & Sons, Chichester, UK, 1988.
[6] T. Frising, P. Leflaive, Microporous Mesoporous Materials 114 (2008) 27–63.
[7] E. Borissenko, F. Porcher, A. Bouché, C. Lecomte, M. Souhassou, Microporous Mesoporous Materials 114 (2008) 155–165.
[8] B.X. Gu, L.M. Wang, R.C. Ewing, Journal of Nuclear Materials 278 (2000) 64–72.
[9] D. Bae, K. Seff, Microporous Mesoporous Materials 33 (1999) 265–280.
[10] C.-C. Chen, K.F. Hayes, Geochimica et Cosmochimica Acta 63 (1999) 3205–3215.
[11] J.K. Reilly, P.J. Grant, G.J. Quinn, T.C. Runion, K.J. Hofstetter, ASTM Special Technical Publication, ASTM, Philadelphia, PA, 1985.
[12] N.F. Chelishchev, in: D.W. Ming, F.A. Mumpton (Eds.), Natural Zeolites'93, International Committee on Natural Zeolites, 1995, pp. 525–532.
[13] National Research Council, A Study of the Isolation System for Geologic Disposal of Radioactive Waste, National Academy Press, Washington, DC, 1983.
[14] L.M. Wang, J. Chen, R.C. Ewing, Current Opinion in Solid State and Materials Science 8 (2004) 405–418.
[15] D.H. Olson, Zeolites 15 (1995) 439–443.

[16] A.P. Hammersley, S.O. Svensson, M. Hanfland, A.N. Fitch, D. Hausermann, High Pressure Research 14 (1996) 235–248.
[17] C. Maurizio, N.E. Habra, G. Rossetto, M. Merlini, E. Cattaruzza, L. Pandolfo, M. Casarin, Chemistry of Materials 22 (2010) 1933–1942.
[18] S.M. Webb, Sam's Interface for XAS Package (SixPACK), Stanford Synchrotron Radiation Laboratory, Menlo Park, CA, 2002.
[19] A.L. Ankudinov, B. Ravel, J.J. Rehr, S.D. Conradson, Physical Review B 58 (1998) 7565–7576.
[20] S. Fendorf, M.J. Eick, P. Grossl, D.L. Sparks, Environmental Science and Technology 31 (1997) 315–320.
[21] G.N. Eby, Principles of Environmental Geochemistry, Thomson Brooks/Cole, Pacific Groove, CA, 2004.
[22] E. Lima, P. Bosch, S. Bulbulian, Applied Radiation and Isotopes 65 (2007) 259–265.
[23] Q. Tang, Q. Zhang, P. Wang, Y. Wang, H. Wan, Chemistry of Materials 16 (2004) 1967–1976.
[24] J.-F. Lee, A.-C. Wei, K.-J. Chao, Journal of Molecular Catalysis A: Chemical 203 (2003) 165–172.
[25] P. Khemthong, W. Klysubun, S. Prayoonpokarach, J. Wittayakun, Materials Chemistry and Physics 121 (2010) 131–137.
[26] A.A. Verberckmoes, B.M. Weckhuysen, R.A. Schoonheydt, Microporous Mesoporous Materials 22 (1998) 165–178.
[27] I.D. Brown, R.D. Shannon, Acta Crystallographica A29 (1973) 266–282.
[28] A.A. Verberckmoes, B.M. Weckhuysen, J. Pelgrims, R.A. Schoonheydt, Journal of Physical Chemistry 99 (1995) 15222–15228.